Title

Tumor resistance to anti-mesothelin CAR-T cells caused by binding to shed mesothelin is overcome by targeting a juxtamembrane epitope

Journal

Proceedings of the National Academy of Sciences of the United States of America, 121(4)

ISSN

0027-8424

Authors

Liu, XF

Onda, M

Schlomer, J

et al.

Publication Date

2024-01-23

DOI

10.1073/pnas.2317283121

PNAS RESEARCH ARTICLE | MICROBIOLOGY OPEN ACCESS

Bacterial flagella hijack type IV pili proteins to control motility

Xiaolin Liu[a,1], Shoichi Tachiyama[b,c,1], Xiaotian Zhou[d], Rommel A. Mathias[d,e], Sharmin Q. Bonny[d], Mohammad F. Khan[d], Yue Xin[d], Anna Roujeinikova[d,e,2], Jun Liu[b,c,2], and Karen M. Ottemann[a,2]

Edited by Jeff Miller, University of California, Los Angeles, CA; received October 8, 2023; accepted November 27, 2023

Bacterial flagella and type IV pili (TFP) are surface appendages that enable motility and mechanosensing through distinct mechanisms. These structures were previously thought to have no components in common. Here, we report that TFP and some flagella share proteins PilO, PilN, and PilM, which we identified as part of the *Helicobacter pylori* flagellar motor. *H. pylori* mutants lacking PilO or PilN migrated better than wild type in semisolid agar because they continued swimming rather than aggregated into microcolonies, mimicking the TFP-regulated surface response. Like their TFP homologs, flagellar PilO/PilN heterodimers formed a peripheral cage that encircled the flagellar motor. These results indicate that PilO and PilN act similarly in flagella and TFP by differentially regulating motility and microcolony formation when bacteria encounter surfaces.

flagellar motor | nanomachine | mechanoresponse

Significance

Bacterial surface appendages, flagella, and type IV pili (TFP) are both reported to sense surfaces, but the mechanisms are not well understood. These organelles operate in different ways—flagella rotate and TFP extend and retract. We used cryo-electron tomography, bacterial genetics, microscopy, and biochemistry to show that flagella have coopted a set of proteins from TFP to form a cage around the flagellar motor. This result was unanticipated, as no one previously knew of proteins shared by these two appendages. These coopted proteins give flagella the ability to regulate activities in addition to motility—adherence, microcolony formation, and biofilm building. The work suggests the surprising idea that surface signaling—detected and transmitted through TFP or flagella—shares conserved features.

Flagellar motility is an important fitness factor for many bacteria and a virulence factor in pathogens. Flagella propel bacteria through liquid and viscous environments using membrane-embedded motors that switch between clockwise and counterclockwise rotation (1–3). The motor powerhouse is a ring of circumferentially positioned stator units that converts the ion-motive force into a turning force (torque) applied to the rotor. While all flagella contain ~20 conserved core components, significant species-to-species variability in the flagellar motor has been recognized (1, 3–5). Motors vary in size, stator unit number, and additional periplasmic structures—disks, rings, and cages (3, 6). For example, *Helicobacter pylori* has a highly complex motor with a large diameter, many accessory disks and rings, and a distinct cage-like structure (7, 8). Such accessories are generally thought to help anchor more stator units, and at a large distance from the axis, to produce higher torque (1, 3, 7). For many motors, the identity of these proteins is unknown, preventing exploration of their function.

H. pylori was recently reported to have three genes that encode distant type IV pili (TFP) homologs of PilO, PilN, and PilM (*SI Appendix*, Fig. S1), arranged in an operon (Fig. 1*A* and *SI Appendix*, Fig. S2) (9, 10). This finding was unexpected, because *H. pylori* does not have TFP or any other identifiable TFP genes. In other bacteria, TFP promote adherence and twitching motility on moist surfaces by repeated extension and retraction (11). PilO, PilN, and PilM are essential components of the TFP cytoplasmic membrane-located alignment subcomplex (12–15). PilM is a cytoplasmic protein and forms dimers by binding its own N terminus (16). PilO and PilN are single-span cytoplasmic membrane proteins with short cytoplasmic domains and substantial periplasmic ones. They exhibit significant sequence homology to each other and form heterodimers and homodimers (13, 17, 18).

Results

***H. pylori* PilO and PilN Repress Motility in Semisolid Agar.** To determine the roles of the remote *H. pylori pilO*, *pilN*, and *pilM* homologs, we deleted each gene singly and in combination and tested the motility of the resultant strains in semisolid agar. In this assay, inoculated bacteria capable of chemotaxis form expanded colonies. Δ*pilO* and Δ*pilN* strains exhibited a significant increase in colony size compared to wild type (WT) after 3 d of incubation, consistent with enhanced migration (Fig. 1*B*). We confirmed this phenotype for *pilO* by complementation (Fig. 1*C*). Expressing *pilO* using a multicopy plasmid, pILL2157 (19), conferred the opposite phenotype to the deletion, with repressed migration compared to WT (Fig. 1*C*). Δ*pilM* did not display different migration from WT at this time point, and the triple mutant Δ*pilMNO* migrated similarly to Δ*pilO* or Δ*pilN* (Fig. 1*B*). Interestingly, results in *SI Appendix*, Fig. S3 showed that the Δ*pilM* mutant has a bigger migration halo than WT after culturing for 2 d, indicating that it retains greater motility than WT, though the diameter of Δ*pilM* mutant halo is much smaller than that of Δ*pilO* or Δ*pilN* mutants. These results suggest that PilM also represses motility of *H. pylori* in semisolid agar, with an effect on motility repression that is less than that of

Author contributions: X.L., S.T., A.R., J.L., and K.M.O. designed research; X.L., S.T., X.Z., R.A.M., S.Q.B., M.F.K., and Y.X. performed research; X.L. contributed new reagents/analytic tools; X.L., S.T., A.R., J.L., and K.M.O. analyzed data; and X.L., S.T., A.R., J.L., and K.M.O. wrote the paper.

The authors declare no competing interest.

This article is a PNAS Direct Submission.

[1]X.L. and S.T. contributed equally to this work.

[2]To whom correspondence may be addressed. Email: anna.roujeinikova@monash.edu, jliu@yale.edu, or ottemann@ucsc.edu.

This article contains supporting information online at https://www.pnas.org/lookup/suppl/doi:10.1073/pnas.2317452121/-/DCSupplemental.

Published January 18, 2024.

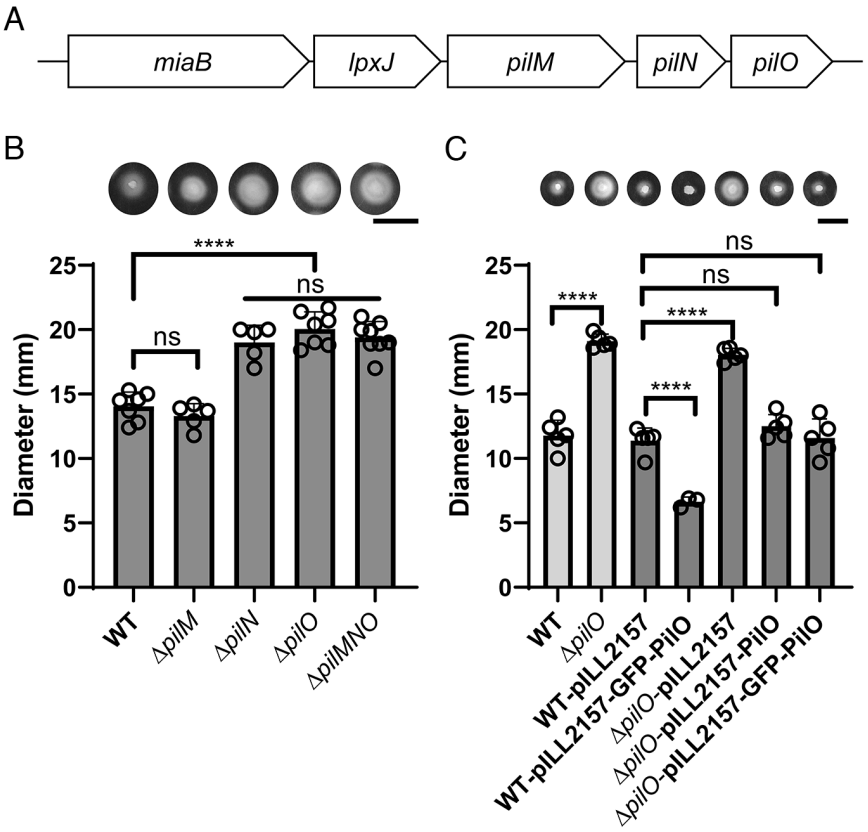

Fig. 1. PilO and PilN repress *H. pylori* migration in semisolid agar. (*A*) Schematic of gene neighborhood encoding MiaB, LpxJ, PilM, PilN, and PilO in *H. pylori*. (*B*) Migration diameter of *H. pylori* WT, Δ*pilM*, Δ*pilN*, Δ*pilO*, and Δ*pilMNO* isogenic mutants in 0.35% (w/v) semisolid agar. The strains were inoculated into semisolid agar media [Brucella broth (BB)-HI-FBS (2.5%), 0.35% agar], and the diameter of the bacterial halo was measured after 3 d. (*C*) Migration diameter of *H. pylori* WT, Δ*pilO* mutant, and derivative strains transformed with pILL2757(empty vector), pILL2157-PilO, or pILL2157-GFP-PilO plasmids, in the same media as panel (*B*) plus 1 mM IPTG. The diameter of each single halo was measured after 3 d. Representative halo pictures are shown in panels (*B*) and (*C*) at the top for each strain. The scale bar indicates 1 cm. Each biological replicate is shown as an open circle, with means obtained from three to six biological replicates. Error bars are SEs. The asterisks indicate a significant pairwise difference between strains according to Student's *t* test. (****$P < 0.0001$; ns, no significant difference.)

PilN and PilO. These findings show that PilM, PilN, and PilO normally have an inhibitory effect on migration in semisolid agar.

It is striking that *pilMNO* are adjacent genes in an operon (9), as *H. pylori* operons often contain genes with unrelated functions. We therefore examined whether this operon is conserved. The distribution of PilO and PilN is widespread (*SI Appendix*, Fig. S4), and the order of *pilMNO* genes is highly conserved, along with the genes *miaB-lpxJ*, in *H. pylori* strains and other Campylobacterota species (*SI Appendix*, Fig. S2). However, even though the *miaB* and *lpxJ* genes occur with *pilMNO*, Δ*miaB* and Δ*lpxJ* showed no differences in migration from WT in semisolid agar (*SI Appendix*, Fig. S5), and deletion of *miaB* or *lpxJ* in the Δ*pilMNO* background phenocopied Δ*pilMNO* (*SI Appendix*, Fig. S5). These results suggest that *miaB* and *lpxJ* products do not act in the same pathway as PilO and PilN.

PilO and PilN Form Heterodimers and Interact with Flagellar Proteins. To understand how PilO and PilN contribute to motility, we fused GFP to the C or N terminus of PilO or PilN and introduced these gene constructs into different strains. Only GFP at the N terminus of PilO was functional, consistent with this end's predicted cytoplasmic location. The lack of functional GFP-PilN is similar to the failure in *Myxococcus xanthus* (20). Complementation of Δ*pilO* with *gfp-pilO* restored migration to WT levels (Fig. 1*C*), suggesting that the fusion of GFP does not impair PilO function. GFP-PilO is located at the cell poles where flagella are (Fig. 2*A* and *SI Appendix*, Fig. S6), leading to the hypothesis that PilO and PilN associate with, or form part of, the flagellar motor. To test this notion, we used quantitative label-free proteomic analysis of proteins that interact (directly or indirectly) with the inner-membrane stator protein MotB. Membrane fractions were isolated and solubilized using mild detergent (digitonin) to preserve protein–protein interactions. Complexes containing MotB were isolated using antibodies and proteins identified by mass spectrometry. By applying a stringent criterion for interaction specificity (>2^6-fold difference in protein amount between the anti-MotB antibody and IgG control), we identified six significant MotB interactions: PilO, PilN, PilM, a FlgX homolog that is a stator-unit chaperone in *Campylobacter jejuni* (21), a hypothetical protein, and MotB's known interaction partner MotA (Fig. 2*B* and *SI Appendix*, Fig. S7). These results indicate that *H. pylori* PilO, PilN and PilM are associated with the flagellar motor.

To gain more insight into PilO interactions, we analyzed the localization of GFP-PilO in diverse backgrounds. PilO retained polar localization in the absence of MotA, MotB, PilM, chemotaxis proteins CheA or CheV1, or flagellar proteins FliL, FlgP, or FlgS (*SI Appendix*, Fig. S6) but lost polar localization in the absence of PilN (Fig. 2*A*). These results show that polar localization of PilO requires PilN, suggesting that both proteins function in vivo as a complex. To test this hypothesis, we co-expressed their C-terminal periplasmic domains with a His_6-tag on one and performed pull-down assays of cell lysates using Ni-NTA affinity chromatography. After co-expression, His_6-PilN-C was co-purified with PilO-C, and His_6-PilO-C was co-purified with PilN-C (Fig. 2*C*). To estimate the PilO-C/PilN-C binding affinity, we prepared

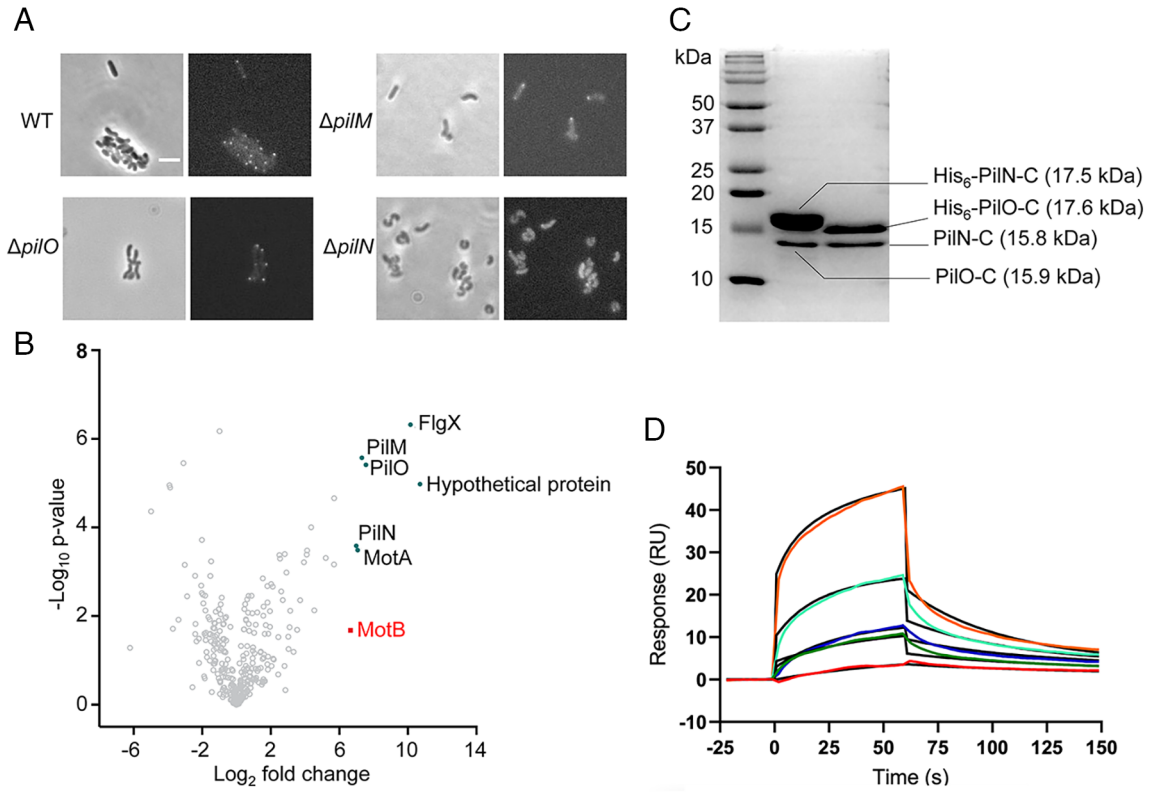

Fig. 2. In vivo and in vitro interactions of PilO with PilN and/or MotB. (*A*) Polar localization of PilO in clusters anchored by PilN. Different *H. pylori* strains (WT, Δ*pilO*, Δ*pilM*, and Δ*pilN*) expressing GFP-PilO from plasmid pILL2157 were imaged using bright-field (*Left*) and fluorescence (*Right*) microscopy. (*B*) Proteomic analysis of immunoaffinity-purified MotB coisolates. Three biological replicates of immunoisolates using anti-MotB antibody or IgG control were compared. Proteins labeled on the volcano plot were significantly enriched (>2^6-fold change) in the anti-MotB antibody sample over the IgG control. Data represent mean values of three biological replicates. (*C*) Co-expression/Ni-NTA co-purification experiment demonstrating that the periplasmic domains of *H. pylori* PilO and PilN form a stable complex. Protein bands on SDS-PAGE gel were identified by mass spectrometry analysis of tryptic peptides. (*D*) Measurements of binding affinity between PilO-C and PilN-C using surface plasmon resonance. Sensograms are representative of two independent experiments. PilN-C concentrations were 7.8 (red), 15.6 (dark green), 31.3 (blue), 62.5 (light green), and 125.0 μM (orange). Data were fit to kinetic model (black line) to estimate the K_D value (K_D = 3.1 ± 1.0 μM).

recombinant PilO-C and PilN-C in isolation and performed surface plasmon resonance measurements of PilN-C binding to PilO-C immobilized on a sensor chip (Fig. 2*D*). Fitting data to a kinetic model yielded the dissociation constant (K_D) value of 3.1 ± 1.0 μM that falls in the middle of the range reported for physiologically relevant protein–protein interactions (22). These data demonstrate that, like their counterparts in TFP, the flagellar motor PilO and PilN associate via their periplasmic domains.

PilO and PilN Constitute Part of the *H. pylori* Flagellar Motor Cage. In TFP, PilO, PilN, and PilM form a round cage-like structure (part of the alignment complex) (12, 20) that encircles the pilus and extends from the cytoplasm, through the inner membrane and into the periplasm (12–15). In *H. pylori*, the flagellar stator ring comprising MotA, MotB, and FliL is also surrounded by a cage structure (7, 8). Drawing on this parallel and our observation of the association between MotB and PilO/N/M, we hypothesized that the *H. pylori* flagellar cage structure comprises PilO, PilN, and PilM. To test this hypothesis, we carried out cryo-electron tomography (cryo-ET) analysis of *H. pylori* mutants lacking *pilM*, *pilN*, *pilO,* or both *pilN* and *pilO* and compared these to the WT flagellar motor. In WT, one end of the cage connects with the outer-membrane disk structure, while the other end passes through the inner membrane (Fig. 3 *A–D*). Loss of *pilO*, *pilN,* or both resulted in loss of parts of the flagellar cage, those in the cytoplasm and proximal to the inner membrane (Fig. 3 *E–H* and *SI Appendix*, Fig. S8 *E–P*). The deletion of *pilM* specifically led to the loss of the cytoplasmic component of the flagellar cage (Fig. 3 *I–L*). To gain further support for the idea that these proteins form the cage, we used AlphaFold2 (23, 24) to predict the *H. pylori* PilO, PilN, and PilM structures (*SI Appendix*, Fig. S9 *A* and *B*) and then docked them into the cryo-ET map. The models of PilO and PilN heterodimers and PilM monomers fit well into the inner-membrane proximal part of the cage density (Fig. 3 *D*, *H*, and *L* and *SI Appendix*, Fig. S9*C*). In addition, we noted that, in comparison to the WT *H. pylori* motor, the densities corresponding to the MotAB complexes and associated FliL rings were not resolved without PilO and/or PilN (Fig. 3 *E* and *F* and *SI Appendix*, Fig. S8 *E–P*) and subtly decreased without PilM (Fig. 3 *I* and *J*). In the motors of other species, e.g., *Escherichia coli* and *Salmonella enterica* (6), the fact that MotAB/FliL densities were not observed by cryo-ET has been attributed to rapid turnover of MotAB subunits (25, 26), possibly as a mechanosensitive response to environmental viscosity (27). These results suggest that the *H. pylori* cage structure, containing PilM/N/O, stabilizes the stator and promotes its full cryo-ET detection, possibly by restraining stator dynamics.

The Cage Represses Motility in Semisolid Agar and Promotes Aggregation into Microcolonies. It was surprising that *H. pylori* mutants lacking PilO or PilN showed better migration in semisolid agar, given that these mutants had stator density invisible in the subtomogram averaged structures compared to WT (Fig. 1*B*). To gain insight into the basis for the better migration, we analyzed swimming speed and chemotaxis response of Δ*pilO* mutants. The Δ*pilO* mutant showed no difference from WT in swimming speed (*SI Appendix*, Fig. S10*A*), reversal frequency (*SI Appendix*, Fig. S10*B*), or chemotaxis response to HCl, a known chemotaxis

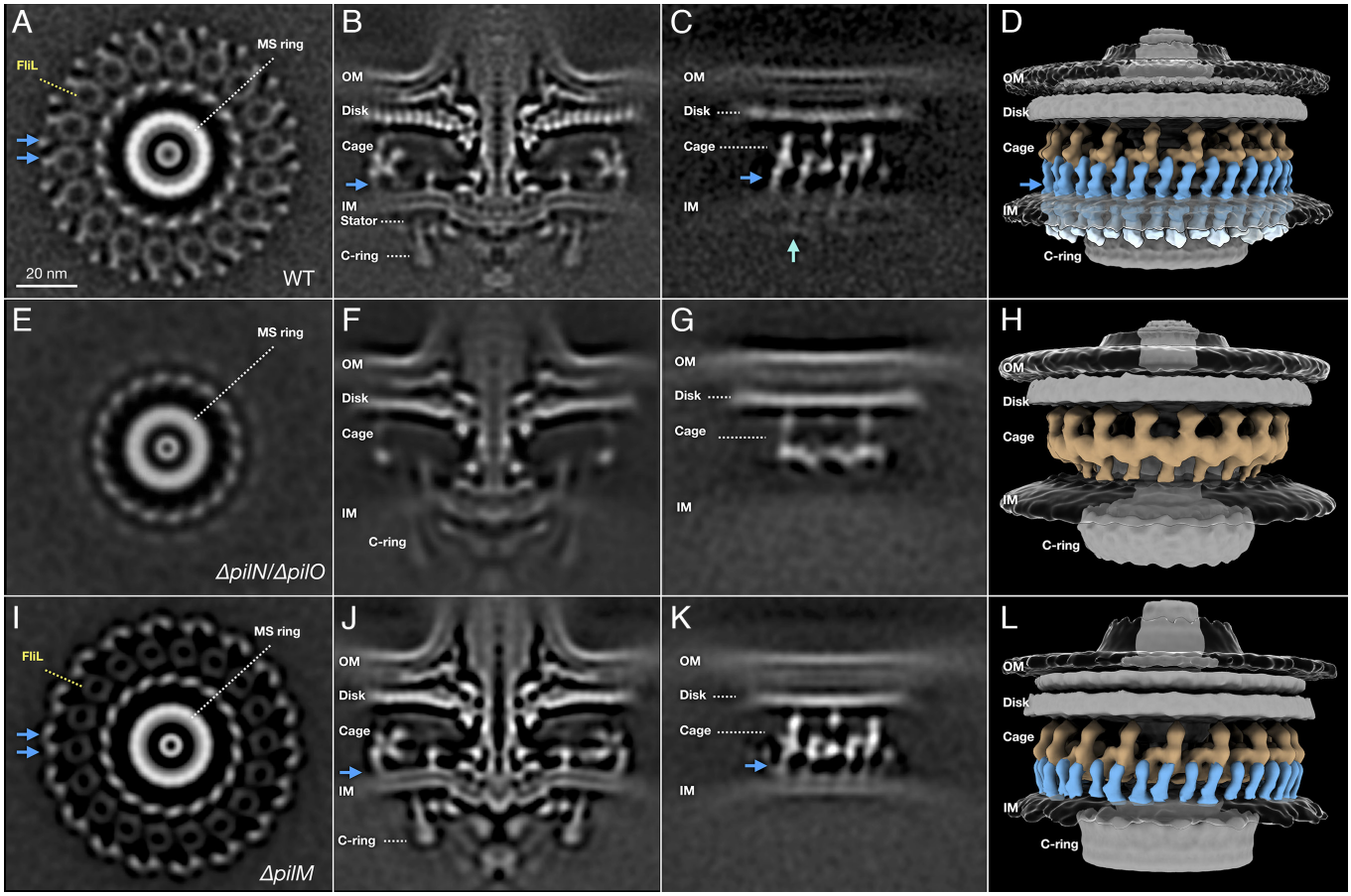

Fig. 3. In situ structures of *H. pylori* flagellar motors reveal that PilN, PilO, and PilM are components of the cage. (*A*) A cross-section of the WT motor structure shows that 18 pairs of two distinct densities (blue arrows) of the cage at the periphery of the FliL circle of rings. (*B*) A medial slice of the WT motor structure. (*C*) A side view of the cage-like structure in the WT motor structure. Globular densities are visible in the cytoplasmic region (light blue arrow). (*D*) An isosurface rendering of the WT motor structure shows the cage-like structure. The outer-membrane-proximal part of the cage is colored in brown, the periplasmic inner-membrane-proximal portion in blue, and the cytoplasmic globular density in light blue. (*E*) A cross section, (*F*) a medial slice, (*G*) a side view of the cage-like structure, and (*H*) an isosurface rendering of the motor in Δ*pilN*/Δ*pilO* mutants. The structure of the motor in Δ*pilN*/Δ*pilO* mutant cells shows that both FliL rings and the entire inner-membrane-proximal portion of the cage are absent. (*I*) A cross section, (*J*) a medial slice, (*K*) a side view of the cage-like structure, and (*L*) an isosurface rendering of the motor in Δ*pilM* mutant cells show that the periplasmic part of the inner-membrane-proximal portion of the cage (blue) is present but the globular densities in the cytoplasmic region are absent.

repellent (28) (*SI Appendix*, Fig. S10*B*). Loss of *pilO* enhanced migration of a variety of *H. pylori* strains, including WT, as well as strains with either counter-clockwise or clockwise flagellar rotation bias (Δ*cheV1*, as reported previously (10), or Δ*cheZ*) (29) (*SI Appendix*, Fig. S11*A*). These results suggested that PilO represses migration of various strains without affecting swimming speed.

We therefore analyzed *H. pylori*'s semisolid agar behavior in more detail. Lack of *pilO* resulted in increased migration that was most enhanced during the first days after inoculation (Fig. 4 *A* and *B*). Specifically, WT *H. pylori* had limited migration for the first 1 to 2 d despite retaining flagella (*SI Appendix*, Fig. S11*B*), while Δ*pilO* mutants migrated immediately (Fig. 4 *A* and *B*). To gain insight into why the WT strain showed slow migration, microscopy analysis was performed on bacteria in semisolid agar. WT *H. pylori* surprisingly formed a high density of microcolonies at these early times, while the Δ*pilO* mutant formed substantially fewer and smaller microcolonies, with a large fraction of the population remaining as single cells (Fig. 4*C*). WT cells were mostly non-motile in the semisolid agar, while Δ*pilO* mutants retained motility (Fig. 4*C* and Movies S1 and S2); both strains were motile in liquid before inserting them into the semisolid agar (Movies S3 and S4). These results indicate that the PilO/N component of the cage enables WT *H. pylori* to stop moving and form aggregates in the semisolid agar. Without the PilO/N cage, *H. pylori* continues to move under semisolid agar conditions and is less able to form microcolonies. Consistent with this idea, Δ*pilO* mutants showed defects in other microcolony-related assays, with less ability to form cell flocs (*SI Appendix*, Fig. S12) and early biofilms (Fig. 4 *D* and *E*).

Semi-solid agar is complex, proposed to contain both elevated viscosity and surfaces (30). To tease these conditions apart, we analyzed the behavior of *H. pylori* WT and Δ*pilO* mutant strains in Ficoll, a highly branched polymer that increases viscosity (31, 32). The addition of Ficoll into liquid media lowered the speed of both WT and the Δ*pilO* mutant, but the Δ*pilO* mutant speed was lowered to a greater extent compared to WT (*SI Appendix*, Fig. S13). This result suggested that some aspect of WT, perhaps the WT form of the stator, is important for the maintenance of a high swimming speed in viscous environments. Importantly, both WT and the Δ*pilO* mutant were still motile, though with low speed, after 1 d of Ficoll incubation (*SI Appendix*, Fig. S13). This response differed from 1 d of incubation in semisolid agar, in which WT lost motility. This difference in response between Ficoll and semisolid agar suggests that viscosity is not a dominant signal in semisolid agar, and the stopping behavior of *H. pylori* in semisolid agar is more consistent with another type of response, perhaps surface contact.

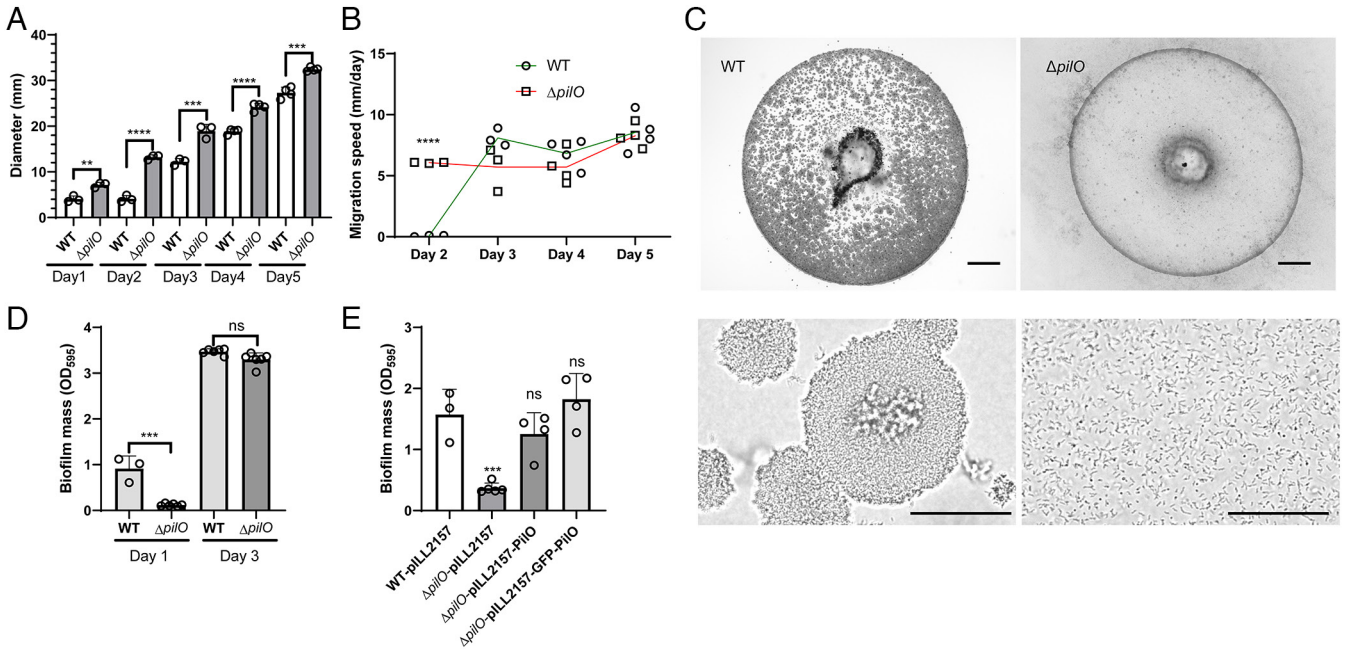

Fig. 4. The cage dampens *H. pylori* motility and promotes microcolony formation on soft agar. (*A*) Time course of *H. pylori* WT and Δ*pilO* migration in 0.35% (w/v) semisolid agar from day 1 to day 5. Strains were inoculated into BB semisolid agar, and the diameter of the migration halo was measured daily. (*B*) Spreading rate of *H. pylori* WT and Δ*pilO* in BB semisolid agar plates from day 2 to day 5. The spreading rate was calculated as the increase in halo diameter per day. (*C*) Representative pictures from BB semisolid agar after 1 d of growth (*Top*) and individual movie frames (*Bottom*) of *H. pylori* WT and Δ*pilO*. WT microcolonies are visible as dense cell aggregates that are absent in Δ*pilO*. The scale bars indicate 500 μm (*Top*) and 50 μm (*Bottom*). (*D* and *E*) Biofilm formation of *H. pylori* WT, Δ*pilO*, and complemented strains under static conditions in microtiter plates after 1 d or 3 d Biofilm formed on the well surface was stained with 0.1% (w/v) crystal violet and quantified by OD_{595}. For strains with plasmids, 1 mM isopropyl-β-D-thiogalactopyranoside (IPTG) was added during the cell culture and biofilm formation. The data are presented as the mean of at least three biological replicates, with each replicate shown as an open circle. Error bars are SEs. The asterisks indicate a significant pairwise difference between strains according to Student's *t* test (***P* < 0.0015; *****P* < 0.0001; ns, no significant difference).

Discussion

Our results show that key components of the cage structure in *H. pylori* flagella are the proteins PilM, PilN, and PilO, homologs of those found in the distinct surface appendage TFP. Our findings also suggest that PilO and PilN do not enhance torque formation or swimming ability but instead repress motility in semisolid agar. Our data are consistent with the notion that PilO, PilN, and PilM act in an outside-in signaling pathway, as reported in *Pseudomonas aeruginosa* TFP, through which PilO controls downstream activity that, in turn, regulates a bacterial surface response (33).

Our data suggest that PilM/N/O regulate the ability of *H. pylori* to stop motility and form microcolonies. Our model is that PilM, PilN, and PilO stop motility under certain conditions. Restricted motility in semisolid agar has been reported as one mechanism causing cell aggregation and microcolonies (34). PilM/N/O possibly are part of a surface-sensing system, though we do not think they sense surfaces directly. PilO of *P. aeruginosa* TFP interacts with the diguanylate cyclase (DGC) SadC and then inhibits its enzymatic activity to reduce the level of c-di-GMP and affect motility and biofilm formation (33). However, different from other bacteria that are used as biofilm models, there are no c-di-GMP-related genes in *H. pylori* genomes, as reported by M. Y. Galperin (35) and confirmed by our own analysis. Additionally, we did not detect any c-di-GMP in *H. pylori* samples under lab conditions using mass spectrometry. These results suggest that *H. pylori* may have a unique mechanism to balance its sessile and motile lifestyles through PilM/N/O, which is independent of c-di-GMP. In *P. aeruginosa*, the DGC SadC, and its product c-di-GMP, bridge TFP and flagellar-derived input signals during initial surface engagement (33). In *H. pylori*, PilO is integrated into the flagellar motor and may interact with the motor directly. In the WT, the stator was visible, while in the Δ*pilN* or Δ*pilO* mutants, the stator was not resolved. Although our cryo-ET data did not allow us to determine whether the unresolved density for the stator was due to its low occupancy or positional or conformational disorder, this finding suggested that the WT cage stabilizes the stator by conformationally restraining it to the extent that it becomes visible in the subtomogram averaged structures. It remains to be established if the cage controls the motor via direct interactions with the stator. Possibilities include that 1) the cage may help recruit stator units by providing additional anchoring points, and thus promote high stator occupancy. 2) the cage may slow down the exchange between the motor and the membrane pool of free stator units. Furthermore, 3) the cage may indeed restrain stator movements in a way that could affect stator function. Our work sets the foundation for future experiments testing these hypotheses.

Flagellar PilM/N/O and TFP PilM/N/O have many similarities. Both flagellar *pilMNO* genes and TFP ones are organized in an operon with the same order. In TFP, PilO and PilN form heterodimers and homodimers (13). In *H. pylori* flagella, PilO and PilN also form heterodimers. Although we did not test PilO or PilN homodimer formation, the expression of PilO only using a multicopy plasmid in the WT background represses motility, a finding that can be explained if PilO in *H. pylori* also forms homodimers, and these are not as active as the PilO–PilN heterodimers. In addition, both flagellar PilM/N/O and TFP PilM/N/O control motility under surface-associated environments. Flagellar PilM/N/O in *H. pylori* are involved in motility repression in the semisolid agar but not in liquid, and TFP are known to be involved in surface-associated twitching motility (33).

Flagellar PilM/N/O and TFP PilM/N/O also have some differences. In TFP, PilM/N/O are important for the assembly and function of TFP (18), while in flagella, they are responsible for the formation of the cage-like structure and are not essential for flagella assembly. In TFP, the deletion of either *pilM*, *pilN*, or *pilO* is

sufficient to abolish the function of TFP. In contrast, flagellar PilM plays a more subtle role compared to PilO and PilN, which have stronger effects on motility repression. There are also differences in bacterial proteins needed for localization. In *M. xanthus* TFP, the PilQ outer membrane secretin recruits the inner membrane lipoprotein PilP that interacts with PilN and PilO directly. The PilP/N/O subcomplex then recruits PilM proteins (36). However, we did not identify remote homologs of PilP or PilQ in *H. pylori* after screening through its genome using a HHpred program (37) nor are these genes part of the flagellar *pilMNO* operon (*SI Appendix*, Fig. S2). Based on our subtomogram averaged structures, PilN/O are close to the *H. pylori* flagellar stator MotA, MotB, and surrounding FliL, but none of these are required for the polar localization of PilO. The possible candidates responsible for recruiting PilO and PilN might be other *H. pylori* flagellar structural components nearby, e.g., the distal periplasmic part of the cage-like structure or the spoke-like structure in the periplasmic region. This idea can only be tested when the components of these structures are identified.

Overall, our results suggest that the *H. pylori* motor has found new ways to modulate its output. We propose a model in which PilO and PilN have been co-opted by flagella yet act like their counterparts in TFP by responding to mechanosensitive input signals to enable microcolony formation (*SI Appendix*, Fig. S14). By hijacking the TFP-like cage structure, *H. pylori* flagella provide both a way to lock flagellar stators in place and a mode of regulatory control that dampens migration and promotes microcolony formation when bacteria encounter surfaces.

Materials and Methods

Detailed materials and methods can be found in *SI Appendix*, Materials and Methods.

Bacterial Strains and Growth Conditions. *H. pylori* WT strains and their derivative mutants used in this study are listed in *SI Appendix*, Table S1. *H. pylori* cells were cultured on solid media consisting of Columbia Horse Blood Agar (CHBA) (Difco), containing: 0.2% (weight/volume) beta-cyclodextrin, 10 μg/mL vancomycin, 5 μg/mL cefsulodin, 2.5 U/mL polymyxin B, 5 μg/mL trimethoprim, and 8 μg/mL amphotericin B (all chemicals are from Thermo Fisher or Gold Biotech), or liquid media consisting of Brucella broth (BB, Difco) with 10% heat-inactivated fetal bovine serum (HI-FBS) (Life Technologies) (BB10). *H. pylori* was cultured at 37 °C under microaerobic conditions of 5% O_2, 10% CO_2, and 85% N_2 with 15 μg/mL kanamycin or 13 μg/mL chloramphenicol. Unless otherwise noted, liquid cultures were shaken at 200 rpm. The *E. coli* DH10B strain used in this study was grown in LB with 15 μg/mL kanamycin.

Semisolid Agar Migration Assay. For the general semisolid agar migration assay, *H. pylori* WT or derivative strains were cultured in liquid BB10 media overnight, in the presence of 1 mM IPTG for strains with pILL2157-derived plasmids. After being adjusted to OD_{600} of 0.15 with fresh BB10 media, the cells were incubated under shaking for 2 h and checked for full motile ability. After cultures displayed high motility, 2 μL was inserted in the center of BB semisolid agar plates composed of BB, 2.5% HI-FBS, and 0.35% (w/v) agar (Bacto). Cells in the semisolid agar were cultured as described above for 1 to 5 d. During the first 2 d, representative bright-field images were captured using a Zeiss AxioImager Z2 widefield microscope with a Zeiss AxioCam 506 (color) camera. For the cells cultured for 2 to 5 d, representative images were taken using a Gel Doc XR+ Gel Documentation System (Biorad). The diameter of the halo in semisolid agar was measured using a default measurement tool in ImageJ (https://imagej.nih.gov/ij/index.html).

Data, Materials, and Software Availability. The WT motor structure (EMD-40405) (38) and the Δ*pilNO* motor structure (EMD-40406) (39) were deposited to the Electron Microscopy Data Bank (EMDB). All other data are included in the manuscript and/or supporting information.

ACKNOWLEDGMENTS. We would like to thank Jashwin Sagoo (UCSC) for useful discussions that framed PilO function, Dr. Nina Salama (Fred Hutchison Cancer Research Center) for providing genomic DNA for several mutant alleles, Dr. Lori Burrows (McMaster University) for helpful discussions about the alignment complex function, Camilla Faoro (Monash University) for assistance with SPR experiments, Naveen Vankadari (Monash University) for preliminary protein preparation work, Samira Heydari (Yale University) for assisting cryo-ET sample preparation and data analyses, and Jennifer Aronson (Yale University) for valuable comments on the manuscript. We thank Dr. Benjamin Abrams at UCSC Life Sciences Microscopy Center, for training and assistance using Zeiss Axio Imager (RRID: SCR_021135), and Dr. Tom Yuzvinsky at UCSC W. M. Keck Center for Nanoscale Optofluidics for assistance using the dual-beam Microscope. The described project was supported by the National Institute of Allergy and Infectious Disease (NIAID) grant R01AI164682 to K.M.O., the Australian Research Council grant DP210103056 to A.R., and a student fellowship from the China Scholarship Council (CSC) 201904910692 to X.L., S.T., and J.L. are supported by the NIAID grants R01AI087846 and R01AI132818. The funders had no role in study design, data collection, or interpretation, or the decision to submit the work for publication.

Author affiliations: [a]Department of Microbiology and Environmental Toxicology, University of California, Santa Cruz, CA 95064; [b]Department of Microbial Pathogenesis, Yale School of Medicine, New Haven, CT 06536; [c]Microbial Sciences Institute, Yale University, West Haven, CT 06516; [d]Infection and Immunity Program, Department of Microbiology, Monash Biomedicine Discovery Institute, Monash University, Clayton, VIC 3800, Australia; and [e]Department of Biochemistry and Molecular Biology, Monash University, Clayton, VIC 3800, Australia

1. X. Zhou, A. Roujeinikova, The structure, composition, and role of periplasmic stator scaffolds in polar bacterial flagellar motors. *Front. Microbiol.* **12**, 639490 (2021).
2. J. P. Armitage, R. M. Berry, Assembly and dynamics of the bacterial flagellum. *Annu. Rev. Microbiol.* **74**, 181–200 (2020).
3. F. M. Rossmann, M. Beeby, Insights into the evolution of bacterial flagellar motors from high-throughput *in situ* electron cryotomography and subtomogram averaging. *Acta Crystallogr. Section D Struct. Biol.* **74**, 585–594 (2018).
4. B. L. Carroll, J. Liu, Structural conservation and adaptation of the bacterial flagella motor. *Biomolecules* **10**, 1492 (2020).
5. S. Subramanian, D. B. Kearns, Functional regulators of bacterial flagella. *Annu. Rev. Microbiol.* **73**, 225–246 (2019).
6. S. Chen *et al.*, Structural diversity of bacterial flagellar motors. *EMBO J.* **30**, 2972–2981 (2011).
7. Z. Qin, W. T. Lin, S. Zhu, A. T. Franco, J. Liu, Imaging the motility and chemotaxis machineries in *Helicobacter pylori* by cryo-electron tomography. *J. Bacteriol.* **199**, e00695-16 (2016), 10.1128/jb.00695-16.
8. S. Tachiyama *et al.*, The flagellar motor protein FliL forms a scaffold of circumferentially positioned rings required for stator activation. *Proc. Natl. Acad. Sci. U.S.A.* **119**, e2118401119 (2022).
9. C. M. Sharma *et al.*, The primary transcriptome of the major human pathogen *Helicobacter pylori*. *Nature* **464**, 250–255 (2010).
10. J. Sagoo, S. Abedrabbo, X. Liu, K. M. Ottemann, Discovery of type IV filament membrane alignment complex homologs in *H. pylori* that promote soft-agar migration. bioRxiv [Preprint] (2023). https://doi.org/10.1101/2023.04.27.537399 (Accessed 27 April 2023).
11. J. M. Skerker, H. C. Berg, Direct observation of extension and retraction of type IV pili. *Proc. Natl. Acad. Sci. U.S.A.* **98**, 6901–6904 (2001).
12. L. Craig, K. T. Forest, B. Maier, Type IV pili: Dynamics, biophysics and functional consequences. *Nat. Rev. Microbiol.* **17**, 429–440 (2019), 10.1038/s41579-019-0195-4.
13. T. L. Leighton, D. H. Yong, P. L. Howell, L. L. Burrows, Type IV pilus alignment subcomplex proteins PilN and PilO form homo- and heterodimers in vivo. *J. Biol. Chem.* **291**, 19923–19938 (2016).
14. S. Tammam *et al.*, Characterization of the PilN, PilO and PilP type IVa pilus subcomplex. *Mol. Microbiol.* **82**, 1496–1514 (2011).
15. T. L. Leighton, M. C. Mok, M. S. Junop, P. L. Howell, L. L. Burrows, Conserved, unstructured regions in Pseudomonas aeruginosa PilO are important for type IVa pilus function. *Sci. Rep.* **8**, 2600 (2018).
16. M. McCallum *et al.*, PilN binding modulates the structure and binding partners of the *Pseudomonas aeruginosa* type IVa pilus protein PilM. *J. Biol. Chem.* **291**, 11003–11015 (2016).
17. L. M. Sampaleanu *et al.*, Periplasmic domains of *Pseudomonas aeruginosa* PilN and PilO form a stable heterodimeric complex. *J. Mol. Biol.* **394**, 143–159 (2009).
18. M. Ayers *et al.*, PilM/N/O/P proteins form an inner membrane complex that affects the stability of the *Pseudomonas aeruginosa* type IV pilus secretin. *J. Mol. Biol.* **394**, 128–142 (2009).
19. I. G. Boneca *et al.*, Development of inducible systems to engineer conditional mutants of essential genes of *Helicobacter pylori*. *Appl. Environ. Microbiol.* **74**, 2095–2102 (2008).
20. Y.-W. Chang *et al.*, Architecture of the type IVa pilus machine. *Science* **351**, aad2001 (2016).
21. D. A. Ribardo, B. R. Kelley, J. G. Johnson, D. R. Hendrixson, A chaperone for the stator units of a bacterial flagellum. *mBio* **10**, e01732-01719 (2019).
22. P. L. Kastritis *et al.*, A structure-based benchmark for protein-protein binding affinity. *Protein Sci.* **20**, 482–491 (2011).
23. J. Jumper *et al.*, Highly accurate protein structure prediction with AlphaFold. *Nature* **596**, 583–589 (2021).

24. M. Mirdita *et al.*, ColabFold: Making protein folding accessible to all. *Nat. Methods* **19**, 679–682 (2022).
25. M. C. Leake *et al.*, Stoichiometry and turnover in single, functioning membrane protein complexes. *Nature* **443**, 355–358 (2006).
26. H. Fukuoka, T. Wada, S. Kojima, A. Ishijima, M. Homma, Sodium-dependent dynamic assembly of membrane complexes in sodium-driven flagellar motors. *Mol. Microbiol.* **71**, 825–835 (2009).
27. P. P. Lele, B. G. Hosu, H. C. Berg, Dynamics of mechanosensing in the bacterial flagellar motor. *Proc. Natl. Acad. Sci. U.S.A.* **110**, 11839–11844 (2013).
28. E. Goers Sweeney *et al.*, Structure and proposed mechanism for the pH-sensing *Helicobacter pylori* chemoreceptor TlpB. *Structure (London, England: 1993)* **20**, 1177–1188 (2012).
29. P. Lertsethtakarn, M. R. Howitt, J. Castellon, M. R. Amieva, K. M. Ottemann, *Helicobacter pylori* $CheZ_{HP}$ and ChePep form a novel chemotaxis-regulatory complex distinct from the core chemotaxis signaling proteins and the flagellar motor. *Mol. Microbiol.* **97**, 1063–1078 (2015).
30. D. B. Kearns, A field guide to bacterial swarming motility. *Nat. Rev. Microbiol.* **8**, 634–644 (2010).
31. N. C. Caiazza, J. H. Merritt, K. M. Brothers, G. A. O'Toole, Inverse regulation of biofilm formation and swarming motility by *Pseudomonas aeruginosa* PA14. *J. Bacteriol.* **189**, 3603–3612 (2007).
32. J. E. Sanfilippo *et al.*, Microfluidic-based transcriptomics reveal force-independent bacterial rheosensing. *Nat. Microbiol.* **4**, 1274–1281 (2019), 10.1038/s41564-019-0455-0.
33. S. S. Webster, C. K. Lee, W. C. Schmidt, G. C. L. Wong, G. A. O'Toole, Interaction between the type 4 pili machinery and a diguanylate cyclase fine-tune c-di-GMP levels during early biofilm formation. *Proc. Natl. Acad. Sci. U.S.A.* **118**, e2105566118 (2021).
34. K. N. Kragh, T. Tolker-Nielsen, M. Lichtenberg, The non-attached biofilm aggregate. *Commun. Biol.* **6**, 898 (2023).
35. M. Y. Galperin, What bacteria want. *Environ. Microbiol.* **20**, 4221–4229 (2018).
36. C. Friedrich, I. Bulyha, L. Søgaard-Andersen, Outside-in assembly pathway of the type IV pilus system in *Myxococcus xanthus*. *J. Bacteriol.* **196**, 378–390 (2014).
37. J. Söding, A. Biegert, A. N. Lupas, The HHpred interactive server for protein homology detection and structure prediction. *Nucleic Acids Res.* **33**, W244–W248 (2005).
38. J. Liu, S. Tachiyama, In situ structure of Helicobacter pylori flagellar motor. Electron Microscopy Data Bank. https://www.ebi.ac.uk/emdb/search/EMD-40405. Deposited 8 April 2023.
39. J. Liu, S. Tachiyama, In situ structure of Helicobacter pylori flagellar motor. Electron Microscopy Data Bank. https://www.ebi.ac.uk/emdb/search/EMD-40406. Deposited 8 April 2023.